Supporting Information

Temperature-Dependent Resonance Energy Transfer from Semiconductor Quantum Wells to Graphene

Young-Jun Yu, Keun Soo Kim, Jungtae Nam, Se Ra Kwon, Hyeryoung Byun, Kwanjae Lee, Jae-Hyun Ryou, Russell D. Dupuis, Jeomoh Kim, Gwanghyun Ahn, Sunmin Ryu, Mee-Yi Ryu and Jin Soo Kim

1. Raman spectra of 4-layer graphene on QWs before and after annealing treatment

Although we transferred multiple-layer graphene on the QWs, the Raman spectrum exhibits a fingerprint of a single-layer graphene (SLG) with the intensity ratio of 0.5 between G and 2D peaks (I_G/I_{2D}), ascribing to the isolation between the stacked graphene layers on QWs as shown in Fig. S1a. Thus, utilizing the annealing process at 250 ^oC in Ar atmosphere (100 sccm) for 2 hours, we removed the polymer residues and stiffened the bonding condition between each stacked graphene layer leading to the fingerprint (I_G/I_{2D} = 2) of the quadruple-layer graphene (QLG), as shown in Fig. S1b. As a result, figure 1b presents the Raman spectra of the different numbers of graphene layers leading to the I_G/I_{2D} ratios of 1, 1.5, and 2 for bi-layer graphene (BLG), triple-layer graphene (TLG), and quadruple-layer graphene (QLG) after the annealing process, respectively. Since the Raman peaks of bare InGaN/GaN QW in Fig. S1c appear at 418.6 cm^{-1}, 569.2 cm^{-1} and 735.4 $cm^{-1}$for sapphire substrate, E_2^H phonon mode and A_1(LO) mode, respectively, there is no overlap between the Raman spectrum of QW and graphene in the range of ~1500 - 3000 cm^{-1}[32, 33]. The Bernal stacking of multilayer graphene has a fingerprint as the 2D Raman peak shows broadening with increasing number of layers. Especially, while the 2D peak of SLG fitted by a single Lorentzian peak is reported as the full width at half maximum (FWHM) of ~ 24 cm^{-1}, the 2D peak of multi-layer graphene from BLG to QLG fitted by multi-Lorentzian peaks exhibits the FWHM of 45-60 cm^{-1} , which is broader than that of SLG [31, 32]. In case of our 2D Raman peaks shown in Fig. 1b, the 2D peaks of SLG, BLG, TLG and QLG on QW, sapphire or SiO_2 substrate are fitted by a single Lorentzian peak with the FWHM of 30~48 cm^{-1} as shown in Fig. S1f, g and h. Although the FWHM extracted from the 2D Raman peaks in Fig. 1b is slightly larger than the reported one, all 2D peaks fitted by a single Lorentzian peak leading

to smaller FWHM than 45 - 60 cm^{-1} allow us to confirm that our multi-layer graphene is not Bernal stacked but randomly stacked.

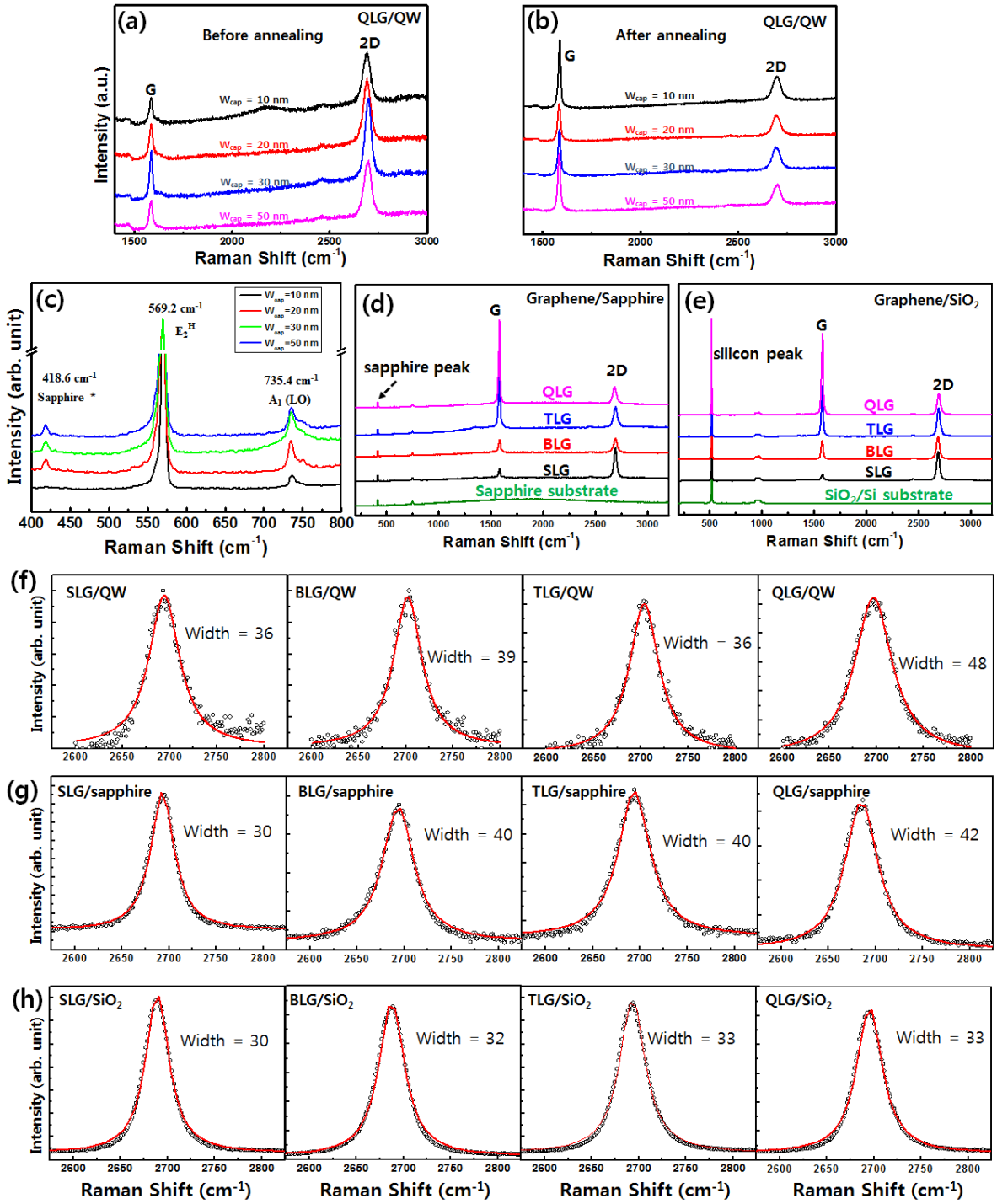

Figure S1. Raman spectra of QLG on QWs (a) before and (b) after annealing treatment. (c) Raman spectra of bare InGaN/GaN QW on sapphire substrate with W_{cap}=10, 20, 30 and 50 nm. Raman spectra of SLG, BLG, TLG and QLG on (d) sapphire substrate and (e) SiO_2

substrate. The single Lorentzian fitted 2D peaks for SLG, BLG, TLG, QLG on (f) QW of Fig. 1b, (g) sapphire substrate of Fig S1d and (h) SiO_2 substrate of Fig S1e.

31. Ferrari, A. C.; Meyer, J. C.; Scardaci, V.; Casiraghi, C.; Lazzeri, M.; Mauri, F.; Piscanec, S.; Jiang, D.; Novoselov, K. S.; Roth, S.; Geim, A. K. Raman spectrum of graphene and graphene layers. *Phys. Rev. Lett.* **2006**, *97*, 187401.

32. Ji, L. W.; Lam, K. T.; Su, Y. K.; Kao, Y. K.; Diao, C. C.; Liao, F. C. Raman study of biaxial strain in InGaN-GaN self assembled quantum dots grown on sapphire(0001). *Inst. Phys. Conf. Ser.* **2004**, *184*, 451-454.

33. Feng, Z. C.; Wang, W.; Chua, S. J.; Zhang, P. X.; Williams, K. P. J.; Pitt, G. D. Raman scattering properties of GaN thin films grown on sapphire under visible and ultraviolet excitation. *J. Raman Spectrosc.* **2001**, *32*, 840-846.

34. Malard, L. M.; Pimenta, M. A.; Dresselhaus, G.; Dresselhaus, M. S. Raman spectroscopy of graphene. *Phys. Rep.* **2009**, *473*, 51-87.

2. Electric doping condition of CVD-SLG.

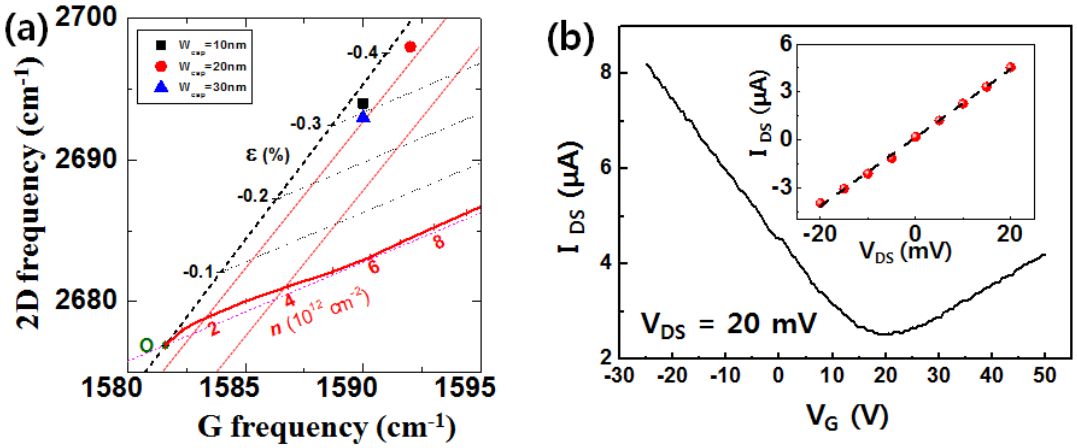

Figure S2. (a) Raman 2D frequency (ω_{2D}) vs. G frequency (ω_G) of SLG on the QWs compared with the origin O(ω_G, ω_{2D}) = (1581.5, 2677) of graphene under natural condition without external influences such as charge impurity and mechanical strain. Regardless of the capping layer thickness (W_{cap}) of the QWs, each SLG on the QWs exhibits the hole-doped condition with a carrier density of n ~ 2.0 × 10^{12} cm^{-2} and compressive strain (-0.3 ≤ ε ≤ -0.4) due to charged residues on the surface and lattice mismatch with the QWs [35]. Here, the effect of mechanical strain by graphene on QWs can be neglected due to the ultrathin graphene thickness (0.3 nm) compared to that of multiple-QWs (> ~100 nm). (b) Current (I_{DS}) variation of SLG on SiO_2 as a function of gate voltage (V_G) while applying bias voltage (V_{DS} = 20 mV). A charge carrier density of n = 1.4×10^{12} cm^{-2} is calculated from n = (C/e)·V_{CNP}, where C, e, and V_{CNP} are capacitance with a value of 12 nF/cm^2 for 300-nm-thick SiO_2, electron charge, and a charge neutral point voltage of ~20 V, respectively. Inset: I_{DS} -V_{DS} characterization curve. Here, the red dots represent the experimental results and the dashed line is a fitted line. To avoid the influence of additional charge carriers during device fabrication such as e-beam lithography and metal contact process, we measured the electron transport characterization of the transferred CVD graphene on SiO_2 substrate using simple two-terminal indium contacts.

35. Lee, J. E.; Ahn, G.; Shim, J.; Lee, Y. S.; Ryu S. Optical separation of mechanical strain from charge doping in graphene. *Nat. Commun.* **2012**, *3*,1024.

3. PL spectra of bare QWs and graphene/QWs with different cap-layer thickness measured at 10 K.

As shown in Fig. S3e, the energy variation of the dominant PL peaks (i.e. effective band gap variation $\Delta E_G = E_{G0} - E_{G1}$) of QWs with different W_{cap} as a function of the number (N) of graphene layers shows a red-shifted trend whereby the ΔE_G increases to ~ 70 meV due to increasing N, where E_{G0} and E_{G1} are the PL energies of bare QW and graphene/QW, respectively. The deviation range of ΔE_G represented by the gray area in Fig. S3e could be calculated from $\Delta E_G = -N \cdot (e \times F \times L_w)$ [37-39] with the electric field (F) from 8 to 120 kV/cm induced by the accumulated charge carrier density from 6×10^{10} to 1.3×10^{12} cm^{-2} on stacked graphene. Here, the electric field F (=V/d) induced by the charge carrier density on graphene can be extracted from $n = (C/e) \times V = (V/d) \times [(\varepsilon \cdot \varepsilon_0)/e]$, where $C = \varepsilon \cdot \varepsilon_0/d$, ε, ε_0, d, and e correspond to the capacitance, dielectric constant of InGaN (ε =14.6) [38, 39], vacuum permittivity, distance for capacitance, and electron charge, respectively. Zhu et al. reported a steady elevation of carrier density at the Dirac point as increasing number of layers. [30] Following this behavior, the gradual escalation of the carrier density in graphene could be expected from SLG leading to 1.3 ~ 2.0×10^{12} cm^{-2} in Fig. S2 and S3 to BLG, TLG and QLG. Thus QLG could be assumed to be in the range of 4.0 ~ 6.0 $\times10^{12}$ cm^{-2} by adding carrier densities of layer by layer of graphene. This indicates that the rearranging Fermi energy level due to the different work functions between hole-accumulated graphene and InGaN/GaN QWs [40-42] results in an increase of the quantum confined Stark effect (QCSE), which causes the reduced band gap of QW.

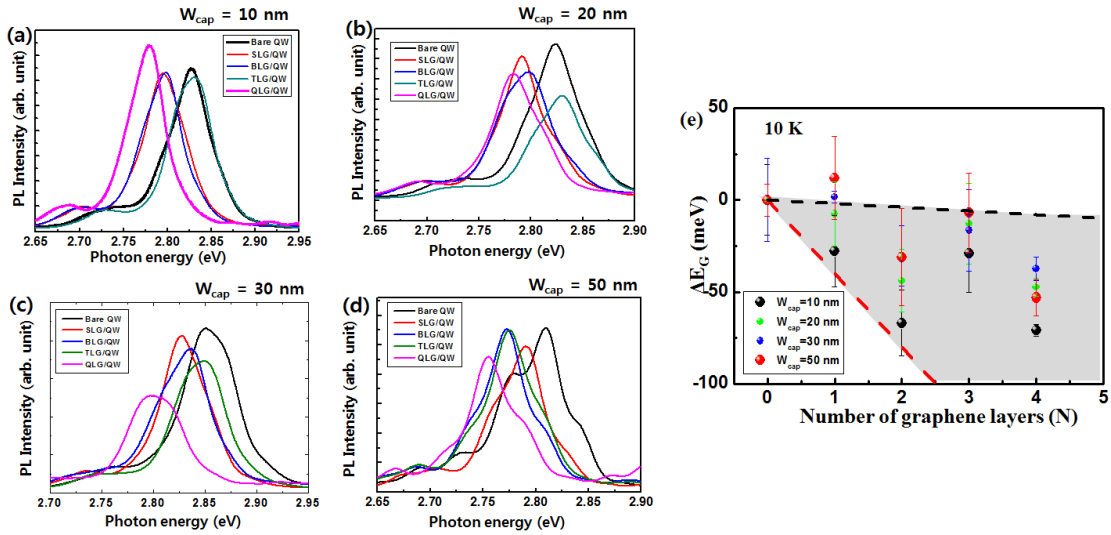

Figure S3. PL spectra of bare QWs, SLG/QW, BLG/QW, TLG/QW, and QLG/QWs with W_{cap}= (a) 10 nm, (b) 20 nm, (c) 30 nm, and (d) 50 nm at 10 K. The PL photon energy is perturbed at around ~2.82 and 2.77 eV as the number of graphene layers escalates from 1 to 4 on QWs with 10, 20, 30, and 50 nm thick cap-layers. However, when we plot the PL photon energy deviation (i.e., band gap variation ΔE_G) as a function of the number of graphene layers, we could observe a red-shifted trend whereby the ΔE_G decreases the amount of ~ 70 meV by escalating the number of graphene layers from 0 to 4 as shown in Fig. 1c. (e) PL peak energies of QWs with different cap-layer thicknesses (10, 20, 30, and 50 nm) as a function of the number of graphene layers (N = 0 - 4). Gray area represents the deviation of ΔE_G decreased by N with black and red dashed boundary lines which are fitted by the electric fields of 8 and 120 kV/cm induced by charge carrier densities of 6×10^{10} and 1.3×10^{12} cm^{-2}, respectively.

30. Zhu, W.; Perebeinos, V.; Freitag, M.; Avouris P. Carrier scattering mobilities, and electrostatic potential in monolayer, bilayer, and trilayer graphene. *Phys. Rev. B* **2009**, *80,* 235402.

37. Hangleiter, A.; Im, J. S.; Off, J.; Scholz, F. Optical properties of Nitride quantum wells: How to separate fluctuations and polarization field effects. *Phys. Stat. Sol.(b)* **1999**, *216,* 427-430.

38. Qian, F.; Brewster, M.; Lim, S. K.; Ling, Y.; Greene, C.; Laboutin, O.; Johnson, J. W.; Gradecak S.; Cao, Y.; Li, Y. Controlled synthesis of AlN/GaN multiple quantum well nanowire structures and their optical properties. *Nano Lett.* **2012**, *12*, 3344-3350.

39. Perlin, P.; Kisielowski, C.; Iota, V.; Weinstein, B. A.; Mattos, L.; Shapiro, N. A.; Kruger, J.; Weber, E. R.; Yang, J. InGaN/GaN quantum wells studied by high pressure, variable temperature, and excitation power spectroscopy. *App. Phys. Lett.* **1998**, *73,* 2778-2780.

40. Yu, Y. -J.; Zhao, Y.; Ryu, S.; Brus, L. E.; Kim, K. S.; Kim, P. Tuning the graphene work function by electric field effect. *Nano Lett.* **2009**, *9,* 3430-3434.

41. Pankove, J. I.; Schade, H. Photoemission from GaN. *App. Phys. Lett.* **1974**, *25*, 53-55.

42. Foresi, J. S.; Moustakas, T. D. Metal contacts to gallium nitride. *App. Phys. Lett.* **1993**, *62*, 2959-2861.

4. Induced quantum confined Stark effect of QW by graphene.

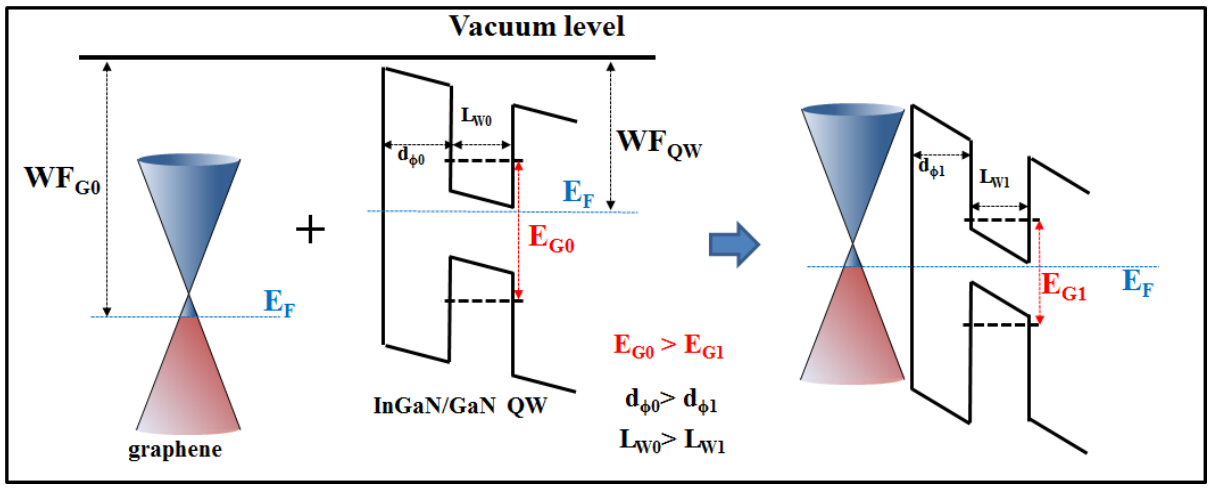

Figure S4. Schematic illustration of the quantum confined Stark effect (QCSE) of QW by covering the hole-doped graphene. WF_{G0}, WF_{QW}, and E_F are the work function of graphene, the work function of QW, and the Fermi energy level, respectively. d_ϕ is the effective barrier distance between QW and graphene that can be extracted by $d_\phi = W_{cap} + L_B$ with W_{cap} = 10, 20, 30, and 50 nm and barrier width (L_B) = 11 nm. The well width (L_W) is 2.5 nm, where d_ϕ, L_W, and energy band gap E_G with subscripts 0 and 1 indicate each value for bare QW and graphene/QW, respectively. Here, the work functions of graphene (WF_{G0}) and QW (WF_{QW}) are employed at ~ 4.6 eV [40] and ~ 4.1 eV [41, 42], respectively.

40. Yu, Y. -J.; Zhao, Y.; Ryu, S.; Brus, L. E.; Kim, K. S.; Kim, P. Tuning the graphene work function by electric field effect. *Nano Lett.* **2009**, *9*, 3430-3434.

41. Pankove, J. I.; Schade, H. Photoemission from GaN. *App. Phys. Lett.* **1974**, *25*, 53-55.

42. Foresi, J. S.; Moustakas, T. D. Metal contacts to gallium nitride. *App. Phys. Lett.* **1993**, *62*, 2959-2861.

5. Temperature dependent PL decay times of QLG/QW and bare QW.

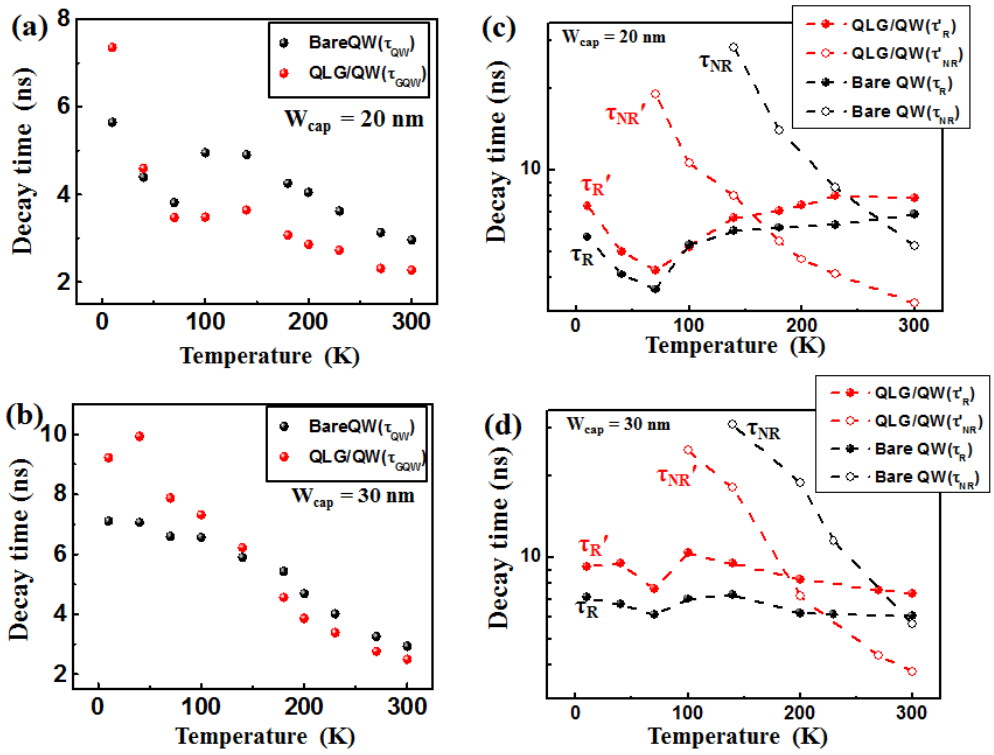

Figure S5. PL decay times of bare QW (τ_{QW}) and QLG/QW (τ_{GQW}) for W_{cap}= (a) 20 nm and (b) 30 nm as a function of T (10 ~ 300 K). (c, d) Radiative and nonradiative recombination times as a function of T extracted from (a) and (b) with $\tau_R = \tau_{QW} \times (I_{10}/I)$, $\tau_{NR} = \tau_{QW} \times (I_{10}/\Delta I)$, $\tau_R' = \tau_{GQW} \times (I_{10}/I)$, and $\tau_{NR}' = \tau_{GQW} \times (I_{10}/\Delta I)$, respectively, where I, I_{10}, and ΔI are the PL intensity at each temperature, PL intensity at 10 K, and PL intensity variation as a function of T, respectively. Here, the time axis is a logarithmic scale.

6. Internal quantum efficiency of QLG/QW and bare QW.

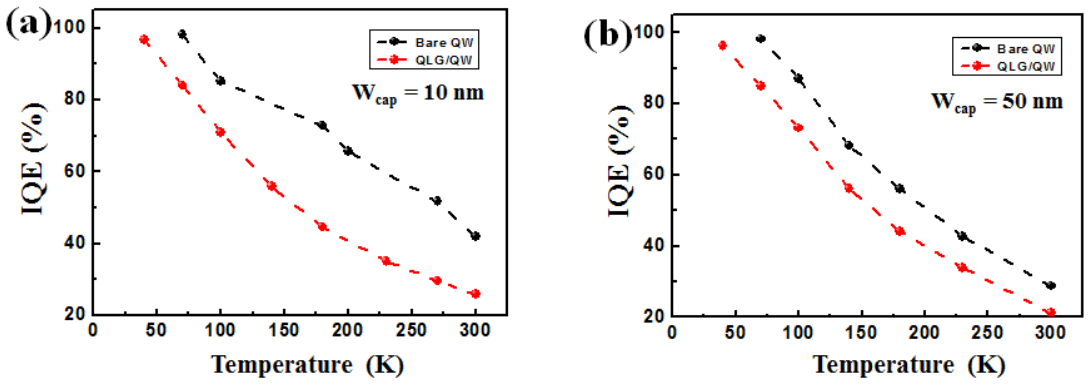

Figure S6. Internal quantum efficiency (IQE) of QLG/QW and bare QW with (a) W_{cap} = 10

nm and (b) 50 nm as a function of T. The IQE can be evaluated using $IQE_{GQW} = \tau_{NR}'/(\tau_R'+\tau_{NR}')$ for QLG/QW and $IQE_{QW} = \tau_{NR}/(\tau_R+\tau_{NR})$ for bare QW, respectively.

7. Energy transfer between QLG and QW under different temperatures

The PL decay time of the bare QW and QLG/QW expressed as $\tau_{QW}^{-1} = \tau_R^{-1} + \tau_{NR}^{-1}$ and $\tau_{GQW}^{-1} = \tau_R^{-1} + \tau_{NR}^{-1} + \tau_{ET}^{-1}$, respectively, leads to $\tau_{ET}^{-1} = \tau_{GQW}^{-1} - \tau_{QW}^{-1}$, where τ_R and τ_{NR} are the radiative and nonradiative decay times, respectively, and τ_{ET} is the characteristic time of the energy transfer process. Thus, the energy transfer efficiency η_{ET} could be expressed as $\eta_{ET} = \tau_{ET}^{-1}/(\tau_{QW}^{-1} + \tau_{ET}^{-1}) = 1 - (\tau_{GQW}/\tau_{QW})$. Upon employing η_{ET} as a function of T, the negative values of η_{ET} are occasionally measured under low T as represented in yellow in Fig. S7. Here η_{ET} as a function of T in Fig. S7a and S7b is yielded with a fast (τ_1) and a slow (τ_2) component from the PL decay curves expressed by a two-exponential function, $A_1 \exp(-t/\tau_1) + A_2 \exp(-t/\tau_2)$, respectively. This might have originated from the supplemented extra carriers to QW from undesirable energy states, such as residues at the interface between graphene and QW or impurities in QW under T < 40 K after the saturation of the excited exciton population in QLG/QW, as extracted IQE in Fig. S6. Even the onset of rapidly increasing τ_{GQW} for W_{cap}=30 nm could also be observed from around 150 K (see also Figs. 1d, S5b and 5d). Therefore, for the RET studies without the unexpected influences in this work, the temperature range was restricted to 40 K ≤ T ≤ 300 K. In addition, the negative value of η_{ET} for W_{cap} = 10, 20, and 30 nm resulting from a longer τ_{GQW} than τ_{QW} as shown in Figs. 2c, S5a and S5b, corresponding to a longer τ_R' than τ_R are overlooked. The neglected area is presented in pink as shown in Fig. S7. Finally, we choose two trends for W_{cap}= (I) 10 nm and (II) 50 nm under 40 K ≤ T ≤ 300 K to discuss the RET behavior shown in Fig. 3.

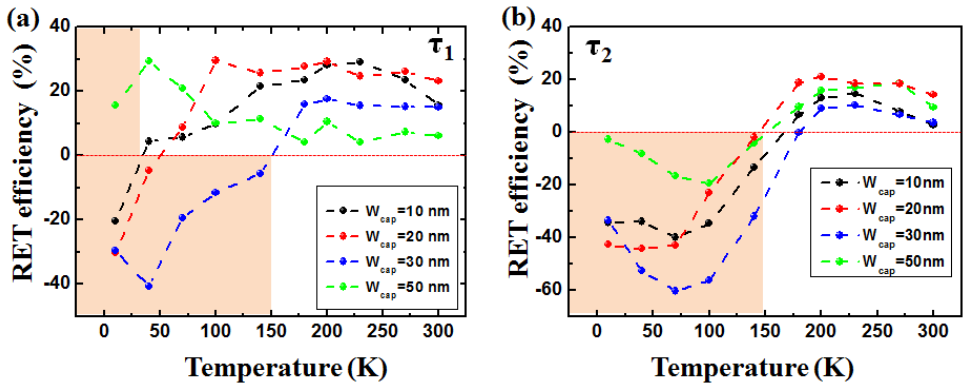

Figure S7. Energy transfer efficiency between QLG and QW extracted with (a) a fast (τ_1) and (b) a slow (τ_2) component from the PL decay curves under different T and cap-layer thickness of W_{cap} = 10, 20, 30 and 50 nm. Here pink area indicates the negative values of η_{ET} ($\tau_{GQW} > \tau_{QW}$) for QLG/QW and T < 40 K for all data.